Atomically Thin Surface Cloak Using Graphene Monolayers

Pai-Yen Chen and Andrea Alù*

Department of Electrical and Computer Engineering, University of Texas at Austin, Austin, Texas 78712, United States

ABSTRACT We discuss here the use of a graphene monolayer to realize the concept of "cloaking by a surface", proposing the thinnest possible *mantle cloak* with operation in the far-infrared and terahertz (THz) regime. We show that an atomically thin graphene monolayer may drastically suppress the scattering of planar and cylindrical objects and, at the same time, preserve moderately broad bandwidth of operation. In addition, we exploit the large tunability of the graphene conductivity to provide active, dynamically tunable invisibility cloaks and versatile THz switching devices.

KEYWORDS: cloaking · graphene · infrared · metamaterials · scattering

In the past few years, tremendous attention has been given to the concept of electromagnetic invisibility cloaks,[1−14] one of the most exciting emerging applications of metamaterials. With the rapid development of metamaterial concepts and the fast evolution of nanofabrication techniques, metamaterial cloaking has been theoretically[1−6,8−10] and experimentally shown[7,11−13] to effectively reduce the overall visibility and scattering of a given object over a wide range of frequencies, spanning from microwaves[7,11] to the infrared and visible spectrum.[12,13] Cloaking technology enables a variety of fascinating applications, including not only invisibility and camouflaging but also noninvasive sensing[5,6] and low-interference communications,[3,16] to name a few. Recently, we have put forward the theoretical idea of using metasurfaces or frequency-selective surfaces (FSS) to realize thin *mantle* cloaks,[14,15] with the advantages of low-cost, moderately broad bandwidth, and easiness of fabrication at microwaves and radio frequencies (RF). The functionality of a mantle cloak essentially relies on the scattering cancellation principle, in some sense analogous to the one of plasmonic cloaks,[1] generating "antiphase" currents on a thin surface that cancel most of the scattered fields from a given object. A thin mantle cloak may be realized at RF by properly patterning a conducting screen, in order to tailor the average surface reactance, providing drastic scattering reduction. For higher frequencies, due to the change in conductivity and finite skin depths of metals at IR and optical frequencies, it is more challenging to practically realize a mantle cloak. In this paper, we extend the notion of "cloaking by a surface" to the far-infrared spectrum, putting forward the idea of the *thinnest possible* surface cloak: an atom thick graphene monolayer, which may realize an infinitesimally thin transverse conductivity layer with suitable values to suppress the scattering of a moderately sized object. We assume in the following an $\exp[-i\omega t]$ time dependence.

RESULTS AND DISCUSSION

Graphene has particularly interesting and unique properties of low-loss surface reactance at far-infrared and terahertz (THz) frequencies,[17,18] ideal for tailoring the induced surface current at will. Its large conductivity over an atom thick layer and its large tunability with respect to the applied bias voltage may provide exciting venues to achieve scattering cancellation effects, even superior to those of RF mantle cloaks. Graphene possesses a truly two-dimensional (2-D) electronic system[19] (effectively a 2-D version of 3-D crystalline graphite), composed of a single atomic layer of carbon atoms arranged in a hexagonal crystal lattice. For this property, the graphene monolayer may be described as a gapless semiconductor, having massless and linear electron−hole dispersion with Fermi velocity $v_F = 10^8$ cm/s. Since the growth of large-area graphene by chemical vapor deposition (CVD)[20] is becoming a mature and standardized process, the anomalous electronic and optical properties of graphene, combined with its extreme thinness, have raised great interest in high-speed electronic[21−24] (*i.e.*, field-effect transistors) and photonic devices[25−33] (*i.e.*, THz oscillators and low noise sensors). In addition, graphene has been theoretically shown to support surface plasmon polarizations in

* Address correspondence to alu@mail.utexas.edu.

Received for review May 3, 2011 and accepted June 12, 2011.

Published online June 12, 2011
10.1021/nn201622e

the infrared spectrum, with relatively low loss and strong wave localization, which have been recently suggested in the realization of transformation metamaterials on an atom thick surface.[17] In the infrared range and below, we can describe the graphene layer with a complex-valued surface conductivity $\sigma_s(\omega) = \sigma'_s - i\sigma''_s$, sensitively dependent on the chemical potential (Fermi energy), which may be largely tuned either *passively* by the doping profile (density and type of carriers[25,27]) or chemical surface modification (*i.e.*, carboxylation and thiolation[35]), or *actively* by external static electric field (providing an isotropic scalar surface conductivity)[25,30] or external static magnetic field *via* Hall effects (providing anisotropic and tensor surface conductivity).[30] Graphene's surface conductivity may be modeled using Kubo formula[27−29]

$$\sigma_s(\omega, \mu_c, \tau, T) = -\frac{ie^2(\omega + i\tau^{-1})}{\pi\hbar^2}\left[\int_{-\infty}^{+\infty} \frac{|\varepsilon|}{(\omega+i\tau^{-1})^2}\frac{\partial f_d(\varepsilon)}{\partial \varepsilon}\,d\varepsilon - \int_0^{+\infty} \frac{\partial f_d(-\varepsilon) - \partial f_d(\varepsilon)}{(\omega+i\tau^{-1})^2 - 4(\varepsilon/\hbar)^2}\,d\varepsilon\right] \quad (1)$$

where $f_d = 1/(1 + \exp[(\varepsilon - \mu_c)/(k_B T)])$ is the Fermi−Dirac distribution, ε is the energy, μ_c is the chemical potential, T is the temperature, e is the electron charge, $\hbar$ is the reduced Planck's constant, and τ is the momentum relaxation time (inverse of the electron−phonon scattering rate), due to the carrier intraband scattering. For simplicity, unless otherwise mentioned, we use here a constant value of $\tau = 0.5$ ps, which is consistent with the ballistic transport features of graphene, whose mean free path was measured to be up to 500 nm at room temperature and larger than 4 μm at low temperature.[23,24] The first term in eq 1 corresponds to the intraband electron−photon scattering process, which can be evaluated as[29]

$$\sigma_{intra} = i\frac{e^2 k_B T}{\pi\hbar^2(\omega + i\tau^{-1})}\left[\frac{\mu_c}{k_B T} + 2\ln\left(\exp\left(-\frac{\mu_c}{k_B T}\right) + 1\right)\right] \quad (2)$$

where the real part of σ_{intra}, associated with τ, contributes to energy absorption or dissipation. The second term corresponds to the direct interband electron transition and, for $\hbar\omega, |\mu_c| \gg k_B T$, and it can be approximated as[29]

$$\sigma_{inter} = i\frac{e^2}{4\pi\hbar}\ln\left[\frac{2|\mu_c| - \hbar(\omega + i\tau^{-1})}{2|\mu_c| + \hbar(\omega + i\tau^{-1})}\right] \quad (3)$$

From eqs 1−3, it is found that, in the THz and far-infrared region, the intraband contribution (eq 2) dominates.[29,34] The unique features of ballistic transport and ultrahigh electron mobility (in excess of 20 000 cm^2 V^{-1} s^{-1})[23] may provide an almost purely imaginary conductivity of graphene in this regime, which can effectively realize a low-loss inductive atomic surface, playing a role analogous to a lossless reactive FSS at RF, without even the need of patterning the surface. This analogy is schematized in Figure 1.

Planar Graphene Cloak. In order to show the potential of making a surface cloak using graphene, we start from a simple 1-D scenario, in which we aim at suppressing the reflection from a planar dielectric slab at the desired frequency. Figure 1 illustrates the proposed graphene surface cloak (right): a graphene monolayer with $\mu_c = 0.13$ eV supported by a silicon dioxide (SiO_2) thin film, with relative permittivity $\varepsilon_{ox} = 3.9$ and thickness $t_{ox} = 1.56\,\mu$m, on top of a dielectric slab, which represents the object to be cloaked, with thickness $d = \lambda_0/5$ and relative permittivity $\varepsilon_d = 5$ (*i.e.*, MgF or KBr). Figure 1 also shows its analogy to a mantle cloak at RF, realized by patterning a conducting surface.[14] The role of the SiO_2 thin film here is to act as a thin spacer for the growth of the graphene monolayer. This 1-D boundary-value problem may be approached using a transmission line model,[15] as sketched in Figure 1, where Z_i and β_i, respectively, represent the characteristic impedance and propagation constant of the ith segment. The dispersive shunt surface impedance Z_s modeling the graphene layer may be obtained from the microscopic quantum dynamic model in eq 2. Here, $Z_s = R_s - iX_s$, where R_s is the surface resistance associated with energy dissipation due to the intraband scattering in graphene (real part in eq 2), which depends mainly on impurities and defects, and X_s is the surface reactance, associated with the imaginary part of eq 2. We assume a room temperature (T = 300 K) operation in the following calculations. Provided that the real part of the input admittance at a given distance t_{ox} from the dielectric slab is equal to the background line admittance $Z_0^{-1} = Y_0 = (377\Omega)^{-1}$, it is possible to suppress the input susceptance by simply adjusting X_s to a suitable value, matching the line and completely canceling the reflected wave at the frequency of interest.

Figure 2a shows the reflectance spectrum for a dielectric slab covered by an ideal lossless mantle cloak with constant reactance X_s = 1248 Ω (red line) and three graphene cloaks (green, orange, and blue lines) with different relaxation times, compared with the uncloaked scenario (dashed line). The graphene cloaks have been designed to suppress the reflection at frequency f_0 = 3 THz ($\hbar\omega_0$ = 12.4 meV), at which the calculated graphene surface impedance is $Z_s = 133 - i1248\ \Omega$ (with a figure of merit $\mathrm{Im}[Z_s]/\mathrm{Re}[Z_s] = 9.38$), as obtained from eq 1. The cloak functionality is verified in Figure 2a, in which it is seen how an atomically thin graphene monolayer may provide significant scattering suppression, analogous to the one of an ideally lossless mantle cloak.[15]

The slight difference between the graphene cloak and an ideal reactive surface is due to the material dispersion and absorption. Even for a relatively short

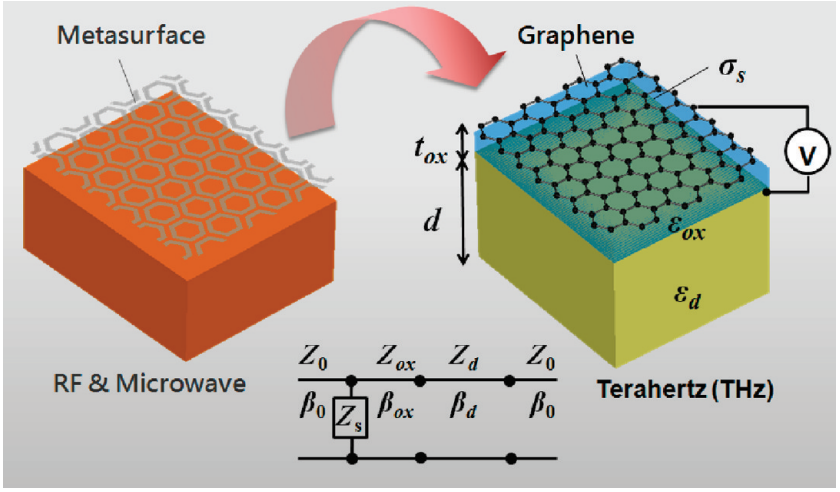

Figure 1. Schematic diagram of (left) a planar mantle cloak realized with a patterned conductor at RF and (right) a graphene surface cloak: an atomically thin graphene monolayer grown on SiO_2. Both geometries may be used to cloak a dielectric planar slab.

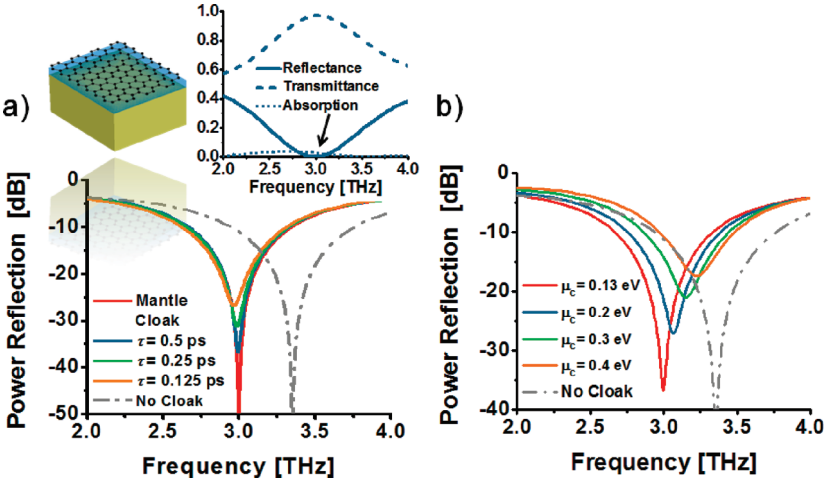

Figure 2. (a) Reflectance spectrum for a $\lambda_0/5$ slab of MgF or KBr ($\varepsilon_d \approx 5$) covered by an ideal mantle cloak with $X_s = 1248\ \Omega$ (red line), a graphene monolayer with $\mu_c = 0.13$ eV loading a 1.56 μm SiO_2 ($\varepsilon_{ox} \approx 3.9$) thin film with different values of τ (blue, green, orange lines), compared with the case without cloak (dashed line). The inset shows the power reflection (solid), absorption (dotted), and transmission (dashed) for the graphene cloak with relaxation time $\tau = 0.5$ ps. (b) Similar to (a), but for different values of chemical potential (here $\tau = 0.5$ ps).

relaxation time $\tau = 0.125$ ps, associated with a larger intraband scattering, a robust cloaking performance is obtained, revealing good robustness against absorption, as is generally true for mantle cloaks.[15] In the uncloaked scenario, the reflection dip at higher frequency is associated with a classic Fabry–Perot resonance. Effectively, the graphene layer can actively tune this reflection dip at the desired frequency, operating in a way similar to an anti-reflection coating but with drastically reduced thickness (one atom thick). The inset of Figure 2a shows the power reflection, absorption, and transmission for the case $\tau = 0.5$ ps. These curves show that indeed the wave is almost completely transmitted through the cloaked slab at the frequency of interest, very different from an absorbing layer, which suppresses the reflection at the price of a large backscattering, in the form of shadow and absence of transmission. This cloaking effect is based on scattering cancellation due to destructive interference between the reflected waves from the graphene layer and the planar slab, and it is therefore effective as long as the object to be cloaked is penetrable and low-loss. This graphene-achieved transparency is also very different from planar carpet cloaking devices,[13] which are designed to cancel the scattering from a bump on a planar reflector, rather than to make the whole reflector transparent.

Effect of Loss and Tunability. To further investigate the influence of intrinsic loss associated with the graphene relaxation time, Figure 3a shows the contours of reflectance gain Q_r, defined as the ratio of power reflection between the cloaked and uncloaked scenarios of

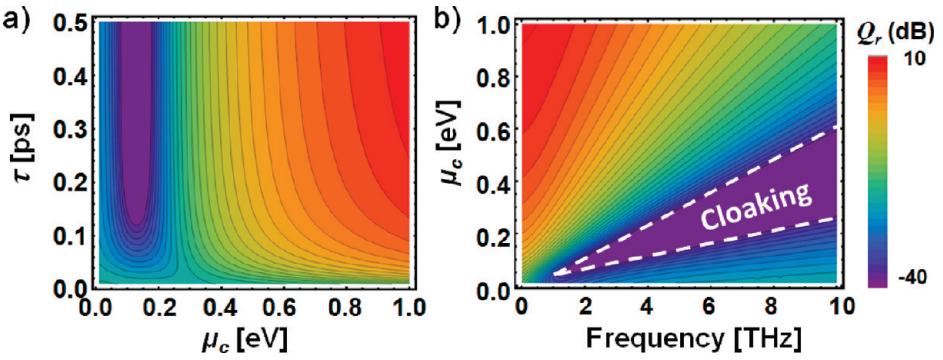

Figure 3. (a) Contours of reflectance gain for the graphene cloak of Figure 2a at the design frequency f_0 = 3 THz, varying chemical potential and relaxation time. (b) Similar contours varying the frequency of operation and chemical potential for τ = 0.5 ps. The cloaking regions are highlighted in the figure.

Figure 2a at the frequency of interest f_0 = 3 THz, varying the chemical potential and relaxation time. The cloaking performance is somewhat deteriorated for very short relaxation times, as expected due to the large intrinsic loss. However, for reasonable values of τ, the cloaking effect is significant and weakly affected by changes in τ. Due to the electron−hole symmetry of the graphene's band structure, both negative and positive signs of chemical potential provide the same complex surface impedance, as well as cloaking performance (see Supporting Information), so we plot in Figure 3 positive values only.

Another advantage of the graphene cloaking layer over classic anti-reflection coatings, in addition to its extreme thinness, is its large tunability. The chemical potential of a graphene layer is determined by the carrier density n_s as[27−28]

$$n_s = \frac{2}{\pi(\hbar v_F)^2}\int_0^\infty \varepsilon[f_d(\varepsilon - \mu_c) - f_d(\varepsilon + \mu_c)]d\varepsilon \quad (4)$$

This implies that a polysilicon gate realized behind the SiO_2 layer may be able to tune and switch the cloaking operation, envisioning the realization of an infinitesimally thin, dynamically tunable THz surface cloak made of graphene and integrated circuitry. A viable way to realize this operation may be a bottom-gate configuration, with the graphene monolayer grown on a SiO_2 insulating layer (spacer). An applied voltage on the polysilicon bottom-gate may tune in real-time the surface electromagnetic properties of graphene. In this scenario, the 2-D surface charge density is controlled by the displacement current on a charged surface $C_{ox}V_g = en_s$, where $C_{ox} = \varepsilon_{ox}\varepsilon_0/t_{ox}$ is the gate capacitance. For instance, in the scenario of Figure 1, we assume a thin gate electrode layer directly behind the SiO_2 spacer (t_{ox} = 1.56 μm). The chemical potential μ_c = 0.13 eV, which corresponds to a carrier density of n_s = 1.36×10^{12} cm^{-2} obtained from eq 4, may be achieved with a gate voltage V_g = 98.6 V, generating a static electric field E_0 = 0.632 MV/cm. We should note that this operation voltage is allowed to be even lower by embedding the gate electrode layer in the SiO_2 spacer with a gate oxide thickness typically less than 0.3 μm. When the applied voltage is increased, more charge will be induced on the graphene surface, which will in turn raise the chemical potential. Typically, the chemical potential may be tuned from −1 to 1 eV by standard values of externally applied bias, as discussed in the Supporting Information.

Figure 2b shows the calculated reflectance varying the graphene's chemical potential from 0.13 up to 0.4 eV. The reflection at the operating frequency may be drastically tuned from "cloaked" (μ_c = 0.13 eV) to "uncloaked" status (μ_c = 0.4 eV). Such behavior is very promising for applications in realizing *actively* tunable cloaks and THz photon switching devices, with a voltage-controllable and electrically driven transparency effect. In this context, Figure 3b shows the reflectance gain contours for the same geometry as in Figure 2 with τ = 0.5 ps and correspondingly optimal t_{ox}, varying the frequency of operation and the graphene chemical potential. It is visible that the frequency of operation can be readily tuned in the THz and far-infrared spectrum by changing the chemical potential. Further discussions on the tunability properties of this technology are provided in the Supporting Information.

Cylindrical Graphene Cloak. Having proven that a single atom thick graphene layer may realize a planar cloak at the desired far-infrared frequency, we extend this concept to a 2-D geometry, envisioning the use of a graphene microtube (or single-walled carbon micro/nanotubes),[36−38] realized by wrapping a graphene monolayer around a seamless cylinder.[19] Here we employ the Lorentz−Mie scattering theory and apply impedance boundary conditions for the graphene conductivity, forcing a discontinuity on the tangential magnetic field distribution on the graphene surface,[14] which is proportional to the induced averaged surface current:

$$\mathbf{H}_{tan}|_{r=a^+} - \mathbf{H}_{tan}|_{r=a^-} = \hat{\mathbf{r}} \times \mathbf{E}_{tan}|_{r=a}/Z_s \quad (5)$$

Details of our analytical solution are provided in the Methods section. We consider an impinging TM polarized plane wave, as illustrated in the inset of Figure 4, which is

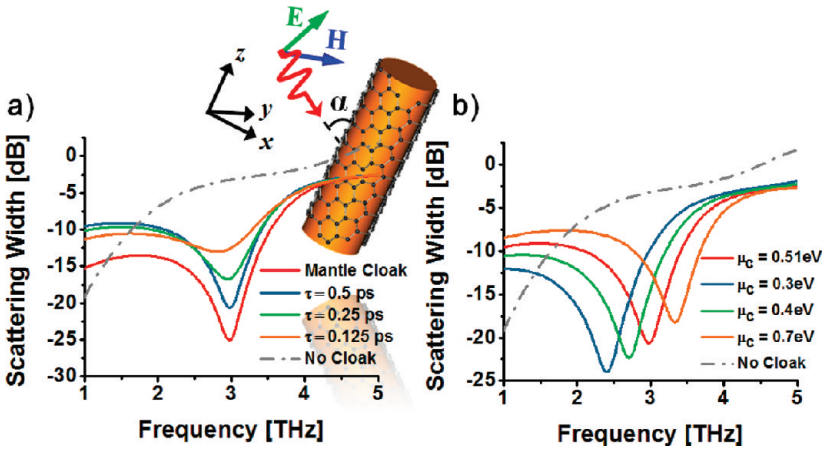

Figure 4. (a) Total SW of an infinite dielectric cylinder with diameter $D = \lambda_0/5$ and relative permittivity $\varepsilon_d = 3.9$, covered by an ideal lossless mantle cloak with surface reactance $X_s = 313\ \Omega$ (red line); graphene surface cloaks with $\mu_c = 0.51$ eV and different values of momentum relaxation time τ (blue, green, and yellow); no cloak (dashed). (b) Similar to (a), but for different graphene chemical potentials and $\tau = 0.5$ ps.

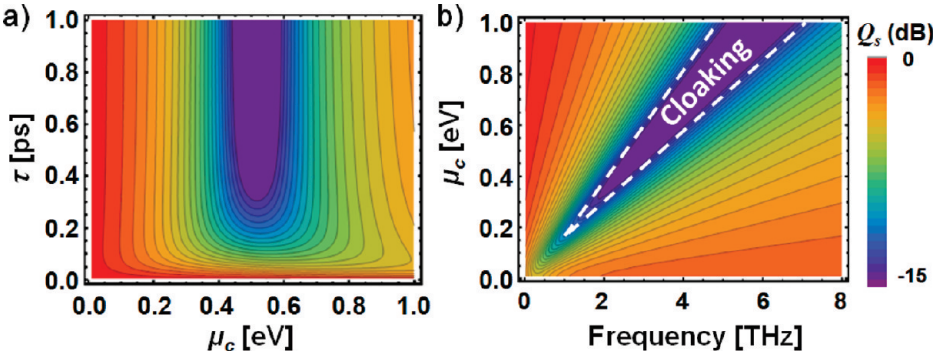

Figure 5. (a) Scattering gain for the graphene cloak of Figure 4a at the frequency of interest $f_0 = 3$ THz, varying chemical potential and momentum relaxation time. (b) Similar plot varying the frequency of operation and chemical potential for $\tau = 0.5$ ps.

the case of most interest for scattering reduction purposes on this geometry. In this case, we calculate the total scattering width (SW),[15,39] as a quantitative measure of its overall visibility, for all angles of observation.

Figure 4a shows the total SW (normalized with respect to wavelength) of an infinite SiO_2 dielectric cylinder with diameter $D = \lambda_0/5$ and relative permittivity $\varepsilon_d = 3.9$ covered by a graphene-wrapped microtube with optimal chemical potential $\mu_c = 0.51$ eV and momentum relaxation time varied from $\tau = 0.5$ to 0.125 ps. We see how significant scattering suppression is achieved at the design frequency $f_0 = 3$ THz using a conformal, atomically thin graphene surface cloak. Good agreement is verified when compared with an ideally lossless 2-D mantle cloak with constant surface reactance $X_s = 313\ \Omega$ (red line). The minor discrepancy between the ideal impedance cloak and the graphene layer is associated with frequency dispersion and absorption (here $Z_s = 33.2 - i313\ \Omega$, with a figure of merit 9.42, is obtained for $\tau = 0.5$ ps; $Z_s = 132.8 - i313\ \Omega$ is obtained for $\tau = 1.25 \times 10^{-13}$ s). The cloaking performance is quite robust to absorption also in this 2-D scenario. Figure 5a shows the contours of scattering gain Q_s, defined as the ratio of scattering width between the cloaked and uncloaked dielectric cylinder in Figure 4a, at the frequency of interest $f_0 = 3$ THz; here we vary the graphene chemical potential and momentum relaxation time. Although the cloaking performance deteriorates with lower relaxation time, for suitable chemical potential, the cloaking effect is relatively robust to losses, being based on a nonresonant scattering cancellation mechanism, similar to plasmonic and mantle cloaking.[15,39,40]

Figure 4b shows the total SW for uncloaked and cloaked cylinders, varying the graphene's chemical potentials from 0.3 to 0.7 eV. The cloaking frequency may be largely tuned by varying the chemical potential, realizing a tunable and switchable cloaking device. At specific frequencies, it is possible to vary the total scattering width by over 2 orders of magnitude, simply through the variation of chemical potential of graphene. This excellent tunability can also be verified in Figure 5b, which shows the contours of scattering gain varying the frequency and chemical potential for $\tau = 0.5$ ps.

Near-Field Distributions. In Figure 6, we show the near-field distributions of the dielectric cylinder

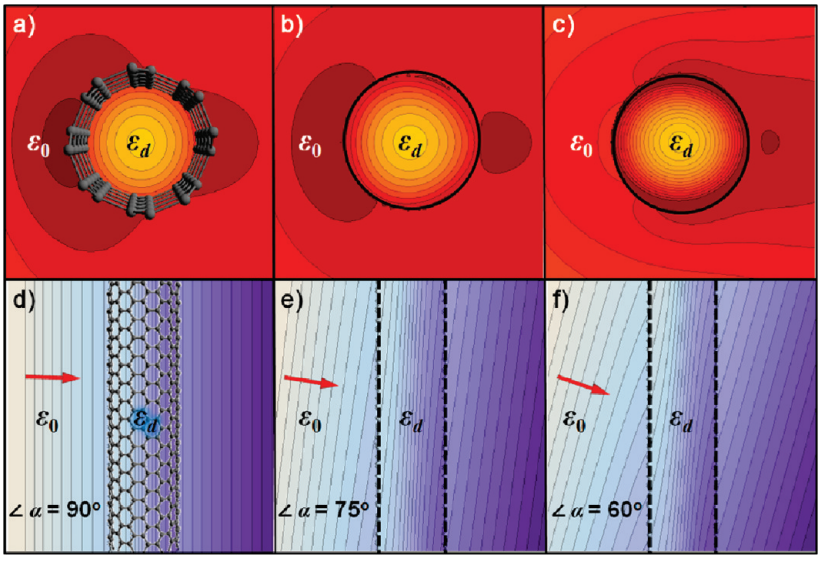

Figure 6. (a–c) Amplitude of the electric field in the *x*–*y* plane (H plane) for an infinite dielectric cylinder covered by a conformal graphene cloak, corresponding to the red line in Figure 4b, at (a) $\alpha = 90°$ (normal incidence), (b) $\alpha = 75°$, and (c) $\alpha = 60°$. (d–f) Similar to (a–c), but for the phase of the magnetic field on the *x*–*z* plane (E plane).

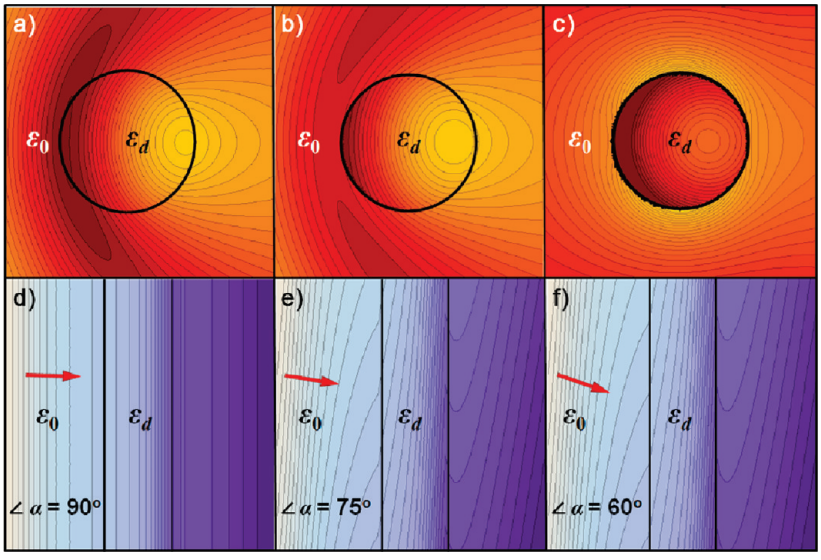

Figure 7. For comparison, similar to Figure 4, but removing the atomically thin graphene layer around the object.

covered by such graphene cloak with $\mu_c = 0.51$ eV and $\tau = 0.5$ ps (red solid line in Figure 4b). The top panels show the electric field amplitude on the H plane at the design frequency $f_0 = 3$ THz for an infinite dielectric cylinder cloaked by a graphene microtube, varying the incidence angle: (a) $\alpha = 90°$ (normal incidence), (b) $\alpha = 75°$, and (c) $\alpha = 60°$ (α is the angle between the incident wave direction and the cylinder axis; see the inset of Figure 4). Bottom panels in Figure 6 show the same contours, but for the phase of the magnetic field on the E plane. It is seen how for both polarizations and all positions around the cylinder, drastic scattering reduction and restoration of the original phase fronts are achieved. For comparison, Figure 7 shows the same plots for the uncloaked dielectric cylinder. In all panels, the plane wave excites the geometry from the left and the corresponding panels in Figures 6 and 7 are plotted on the same color scale for fair comparison. It is visible that the graphene surface cloak has the remarkable property of drastically suppressing the scattering even right around its surface in the very near-field of the object. In contrast to the cloaked case, the uncloaked cylinder highly perturbs the impinging wave, due to much stronger scattering. It is also worth noting that, similar to the plasmonic cloaking technique,[1,3] the wave penetrates the graphene cloak and the cloaked object, thereby enabling applications as cloaked sensors,[3] noninvasive probing, and low-interference communications in the THz regime.

CONCLUSIONS

We have proposed here the concept and potential realization of an atomically thin surface cloak using graphene at THz frequencies. We have shown that the conductivity properties of a single atom thick graphene layer may have exciting applications in suppressing the scattering from moderately sized objects. We have studied the scattering properties of graphene-covered planar and cylindrical objects, accurately modeling the dispersive surface impedance (conductivity) of graphene, as derived from microscopic quantum dynamic models. Graphene has a great potential to realize the ultimately thin cloak at THz frequencies, somehow filling the THz gap for scattering-cancellation cloaks between *mantle cloaks* realized with conducting metasurfaces[14] at RF and *plasmonic cloaks* in the visible.[1] The highly tunable conductive properties of graphene may provide exciting venues to apply these concepts to dynamically tunable THz devices and noninvasive probes and sensors.

METHODS

In this section, we provide analytical expressions for the scattering from an infinite cylinder with radius a covered by a mantle cloak with radius a_c under arbitrary wave illumination in free space. Applying the well-known Lorentz−Mie scattering theory,[41,42] a given monochromatic electromagnetic wave, propagating in a background material with permittivity ε_0 and permeability μ_0 and impinging on a scatter centered at the origin of a cylindrical coordinate system, may always be expanded as a superposition of orthogonal cylindrical harmonics as[42]

$$\begin{aligned} \mathbf{E}_i &= \sum_{n=-\infty}^{\infty} a_n \nabla \times \nabla \times (z\varphi_n) \\ \mathbf{H}_i &= -i\omega\varepsilon_0 \sum_{n=-\infty}^{\infty} a_n \nabla \times (z\varphi_n) \end{aligned} \tag{6}$$

and the scattered fields may be similarly represented by

$$\begin{aligned} \mathbf{E}_s &= \sum_{n=-\infty}^{\infty} c_n^{\mathrm{TM}} a_n \nabla \times \nabla \times (\mathbf{z}\varphi_n) + i\omega\mu_0 \sum_{n=-\infty}^{\infty} c_n^{\mathrm{TE}} b_n \nabla \times (\mathbf{z}\varphi_n) \\ \mathbf{H}_s &= \sum_{n=-\infty}^{\infty} c_n^{\mathrm{TE}} b_n \nabla \times \nabla \times (\mathbf{z}\varphi_n) - i\omega\varepsilon_0 \sum_{n=-\infty}^{\infty} c_n^{\mathrm{TM}} a_n \nabla \times (\mathbf{z}\varphi_n) \end{aligned} \tag{7}$$

where $\mathbf{z}$ is the unit vector along the cylinder axis and φ_n is scalar cylindrical harmonics,[42] solutions of the Helmholtz equation in the cylindrical coordinate systems. The coefficients a_n and b_n are, respectively, the amplitudes of the expanded impinging wave in terms of electric and magnetic multipoles of order n, respectively, and the scattering coefficients c in eq 7 relate the scattered fields to the impinging ones. The unknown scattering coefficients may be obtained by matching the tangential field components according to eq 5, and after some manipulations, they may be expressed as a function of eight-by-eight determinants:

$$c_n^{\mathrm{TM}} = -\frac{U_n^{\mathrm{TM}}}{U_n^{\mathrm{TM}} + iV_n^{\mathrm{TM}}}, \quad c_n^{\mathrm{TE}} = -\frac{U_n^{\mathrm{TE}}}{U_n^{\mathrm{TE}} + iV_n^{\mathrm{TE}}} \tag{8}$$

where U_n^{TM}, V_n^{TM}, U_n^{TE}, and V_n^{TE} have generalized expressions:

$$U_n^{\mathrm{TM}}(\alpha) = \begin{vmatrix} J_n(k^{\mathrm{T}}a) & J_n(k_0^{\mathrm{T}}a) & Y_n(k_0^{\mathrm{T}}a) & 0 \\ \frac{k}{k^{\mathrm{T}}\eta}J_n'(k^{\mathrm{T}}a) & \frac{k_0}{k_0^{\mathrm{T}}\eta_0}J_n'(k_0^{\mathrm{T}}a) & \frac{k_0}{k_0^{\mathrm{T}}\eta_0}Y_n'(k_0^{\mathrm{T}}a) & 0 \\ 0 & J_n(k_0^{\mathrm{T}}a_c) & Y_n(k_0^{\mathrm{T}}a_c) & J_n(k_0^{\mathrm{T}}a_c) \\ 0 & \frac{k_0}{k_0^{\mathrm{T}}\eta_0}Z_sJ_n'(k_0^{\mathrm{T}}a_c) + iJ_n(k_0^{\mathrm{T}}a_c) & \frac{k_0}{k_0^{\mathrm{T}}\eta_0}Z_sY_n'(k_0^{\mathrm{T}}a_c) + iY_n(k_0^{\mathrm{T}}a_c) & \frac{k_0}{k_0^{\mathrm{T}}\eta_0}Z_sJ_n'(k_0^{\mathrm{T}}a_c) \end{vmatrix} \tag{9}$$

$$V_n^{\mathrm{TM}}(\alpha) = \begin{vmatrix} J_n(k^{\mathrm{T}}a) & J_n(k_0^{\mathrm{T}}a) & Y_n(k_0^{\mathrm{T}}a) & 0 \\ \frac{k}{k^{\mathrm{T}}\eta}J_n'(k^{\mathrm{T}}a) & \frac{k_0}{k_0^{\mathrm{T}}\eta_0}J_n'(k_0^{\mathrm{T}}a) & \frac{k_0}{k_0^{\mathrm{T}}\eta_0}Y_n'(k_0^{\mathrm{T}}a) & 0 \\ 0 & J_n(k_0^{\mathrm{T}}a_c) & Y_n(k_0^{\mathrm{T}}a_c) & Y_n(k_0^{\mathrm{T}}a_c) \\ 0 & \frac{k_0}{k_0^{\mathrm{T}}\eta_0}Z_sJ_n'(k_0^{\mathrm{T}}a_c) + iJ_n(k_0^{\mathrm{T}}a_c) & \frac{k_0}{k_0^{\mathrm{T}}\eta_0}Z_sY_n'(k_0^{\mathrm{T}}a_c) + iY_n(k_0^{\mathrm{T}}a_c) & \frac{k_0}{k_0^{\mathrm{T}}\eta_0}Z_sY_n'(k_0^{\mathrm{T}}a_c) \end{vmatrix} \tag{10}$$

$$U_n^{\mathrm{TE}}(\alpha) = \begin{vmatrix} \frac{k\eta}{k^{\mathrm{T}}}J_n'(k^{\mathrm{T}}a) & \frac{k_0\eta_0}{k_0^{\mathrm{T}}}J_n'(k_0^{\mathrm{T}}a) & \frac{k_0\eta_0}{k_0^{\mathrm{T}}}Y_n'(k_0^{\mathrm{T}}a) & 0 \\ J_n(k^{\mathrm{T}}a) & J_n(k_0^{\mathrm{T}}a) & Y_n(k_0^{\mathrm{T}}a) & 0 \\ 0 & J_n'(k_0^{\mathrm{T}}a_c) & Y_n'(k_0^{\mathrm{T}}a_c) & J'(k_0^{\mathrm{T}}a_c) \\ 0 & \frac{k_0\eta_0}{k_0^{\mathrm{T}}}J_n'(k_0^{\mathrm{T}}a_c) + iZ_sJ_n(k_0^{\mathrm{T}}a_c) & \frac{k_0\eta_0}{k_0^{\mathrm{T}}}Y_n'(k_0^{\mathrm{T}}a_c) + iZ_sY_n(k_0^{\mathrm{T}}a_c) & iZ_sJ_n(k_0^{\mathrm{T}}a_c) \end{vmatrix} \tag{11}$$

$$V_n^{TE}(\alpha) = \begin{vmatrix} \frac{k\eta}{k^T}J_n'(k^Ta) & \frac{k_0\eta_0}{k_0^T}J_n'(k_0^Ta) & \frac{k_0\eta_0}{k_0^T}Y_n'(k_0^Ta) & 0 \\ J_n(k^Ta) & J_n(k_0^Ta) & Y_n(k_0^Ta) & 0 \\ 0 & J_n'(k_0^Ta_c) & Y_n'(k_0^Ta_c) & Y'(k_0^Ta_c) \\ 0 & \frac{k_0\eta_0}{k_0^T}J_n'(k_0^Ta_c)+iZ_sJ_n(k_0^Ta_c) & \frac{k_0\eta_0}{k_0^T}Y_n'(k_0^Ta_c)+iZ_sY_n(k_0^Ta_c) & iZ_sY_n(k_0^Ta_c) \end{vmatrix} \quad (12)$$

$J_n(\cdot)$ and $Y_n(\cdot)$ are the cylindrical Bessel function of the first and second kind of order n,[43] $k_i^T = (k_i^2 - \beta^2)^{1/2}$ is the transverse wavenumber, $\beta = k_0 \cos\alpha$ is the wavenumber component along the cylinder axis, and $k_0^T = k_0 \sin\alpha$ is expected (α is the angle between the incident wave direction and the cylinder axis; see the inset of Figure 4). Under an impinging TM_z-polarized wave, the total scattering width (SW), as a quantitative measure of the overall visibility of the cylinder at the frequency of interest, is given by the formula[41]

$$\sigma_s = \frac{4}{k_0}\sum_{n=-\infty}^{n=\infty}|c_n^{TM}|^2 + |c_n^{TE}|^2 \quad (13)$$

In order to suppress the dominant nth TM (TE) cylindrical scattering harmonic for an infinite dielectric cylinder ($\varepsilon > \varepsilon_0$, $\mu = \mu_0$), thus reducing the visibility of the cloaked object, the determinants U_n^{TM} (U_n^{TE}) in eq 8 must be canceled. It is instructive to analyze eq 8 in the quasi-static limit of small objects, for which k_0a, $ka \ll 1$. In such scenario, the dominant coefficients contributing to the scattering of a dielectric cylinder are given by c_0^{TM} and c_1^{TE} in eq 8 and the approximate conditions for cloaking two polarizations can be written in explicit forms. The optimal surface reactance, achieving near-zero total scattering, in the isotropic scenario is given by

$$X_s = \frac{2}{\omega a\gamma\varepsilon_0(\varepsilon-1)} + \frac{\omega a\mu_0((\gamma^2-1)\sin^2\alpha)}{4\gamma^3(\varepsilon-1)} \approx \frac{2}{\omega a\gamma\varepsilon_0(\varepsilon-1)} \quad (14)$$

The quasi-static expression 14 ensures that the incidence angle only weakly affects the cloaking performance, a fact that has been indeed verified with our full-wave simulations in the graphene cloaks analyzed in this study. Similar robustness was verified for plasmonic cloaks in ref 39. If the electrical size of object becomes larger, dynamic formulas 9–12 should be used for the proper design of surface cloaks.

Acknowledgment. This work has been partially supported by AFOSR with the YIP Award No. FA9550-11-1-0009, by NSF with the CAREER Award No. ECCS-0953311, and by the ONR MURI grant No. N00014-10-1-0942.

Supporting Information Available: Tunability of the surface impedance properties of a graphene monolayer. This material is available free of charge via the Internet at http://pubs.acs.org.

REFERENCES AND NOTES

1. Alù, A; Engheta, N. Achieving Transparency with Plasmonic and Metamaterial Coatings. *Phys. Rev. E* **2005**, *72*, 016623.
2. Alù, A.; Engheta, N. Multifrequency Optical Invisibility Cloak with Layered Plasmonic Shells. *Phys. Rev. Lett.* **2008**, *100*, 113901.
3. Alù, A.; Engheta, N. Cloaking a Sensor. *Phys. Rev. Lett.* **2009**, *102*, 233901.
4. Silveririnha, M. G.; Alù, A.; Engheta, N. Infrared and Optical Invisibility Cloak with Plasmonic Implants Based on Scattering Cancellation. *Phys. Rev. B.* **2008**, *78*, 075107.
5. Alù, A.; Engheta, N. Cloaked Near-Field Scanning Optical Microscope Tip for Noninvasive Near-Field Imaging. *Phys. Rev. Lett.* **2010**, *105*, 263906.
6. Bilotti, F.; Tricarico, S.; Pierini, F.; Vegni, L. Cloaking Apertureless Near-Field Scanning Optical Microscopy tips. *Opt. Lett.* **2011**, *36*, 211–213.
7. Edward, B.; Alù, A; Silverinha, M. G.; Engheta, N. Experimental Verification of Plasmonic Cloaking at Microwave Frequencies with Metamaterials. *Phys. Rev. Lett.* **2009**, *102*, 153901.
8. Nicorovici, N. A. P.; Milton, G. W.; McPhedran, R. C.; Botten, L. C. Quasistatic Cloaking of Two-Dimensional Polarizable Discrete Systems by Anomalous Resonance. *Opt. Express* **2007**, *15*, 6314–6323.
9. Tretyakov, S.; Alitalo, P.; Luukkonen, O.; Simovski, C. Broadband Electromagnetic Cloaking of Long Cylindrical Objects. *Phys. Rev. Lett.* **2009**, *103*, 103905.
10. Pendry, J. B.; Schurig, D.; Smith, D. R. Controlling Electromagnetic Fields. *Science* **2006**, *312*, 1780–1782.
11. Schurig, D.; Mock, J. J.; Justice, B. J.; Cummer, S. A.; Pendry, J. B.; Starr, A. F.; Smith, D. R. Metamaterial Electromagnetic Cloak at Microwave Frequencies. *Science* **2006**, *314*, 977–980.
12. Valentine, J.; Li, J.; Zentgraf, T.; Bartal, G.; Zhang, X. An Optical Cloak Made of Dielectrics. *Nat. Mater.* **2009**, *8*, 568–571.
13. Ergin, T.; Stenger, N.; Brenner, P.; Pendry, J. B.; Wegener, M. Three-Dimensional Invisibility Cloak at Optical Wavelengths. *Science* **2010**, *328*, 337–339.
14. Alù, A. Mantle Cloak: Invisibility Induced by a Surface. *Phys. Rev. B* **2009**, *80*, 245115.
15. Chen, P. Y.; Alù, A. Patterned Metallic Surfaces To Realize 1-D, 2-D, and 3-D Ultrathin Invisibility Cloaks. *IEEE International Symposium on Antennas and Propagation*; Toronto, Canada, July 11–17, 2010.
16. Kwon, D. H.; Werner, D. H. Restoration of Antenna Parameters in Scattering Environments Using Electromagnetic Cloaking. *Appl. Phys. Lett.* **2008**, *92*, 113507.
17. Vakil, A.; Engheta, N. Transformation Optics Using Graphene. *Science* **2011**, *332*, 1291–1294.
18. Jablan, M.; Buljan, H.; Sojačić, M. Plasmonics in Graphene at Infrared Frequencies. *Phys. Rev. B* **2009**, *80*, 245435.
19. Geim, A. K.; Novoselov, K. S. The Rise of Graphene. *Nat. Mater.* **2007**, *6*, 183–191.
20. Bae, S.; Kim, H.; Lee, Y.; Xu, X.; Park, J. S.; Zheng, Y.; Balakrishnan, J.; Lei, T.; Kim, H. R.; Song, Y. I. *et al.* Roll-to-Roll Production of 30-in. Graphene Films for Transparent Electrodes. *Nat. Nanotechnol.* **2010**, *5*, 574–578.
21. Lin, Y. M.; Jenkins, K. A.; Valdes-Garcia, A.; Small, J. P.; Farmer, D. B.; Avouris, P. Operation of Graphene Transistors at Gigahertz Frequencies. *Nano Lett.* **2009**, *9*, 422–426.
22. Xia, F.; Farmer, B. B.; Lin, Y.; Avouris, P. Graphene Field-Effect Transistors with High On/Off Current Ratio and Large Transport Band Gap at Room Temperature. *Nano Lett.* **2010**, *10*, 715–718.
23. Bolotin, K. I.; Sikesb, K. J.; Jianga, Z.; Klimac, M.; Fudenberga, G.; Honec, J.; Kima, P.; Stormera, H. L. Ultrahigh Electron Mobility in Suspended Graphene. *Solid State Commun.* **2008**, *145*, 351–355.
24. Mann, D.; Javey, A.; Kong, J.; Wang, Q.; Dai, H. Ballistic Transport in Metallic Nanotubes with Reliable Pd Ohmic Contacts. *Nano Lett.* **2003**, *3*, 1541–1544.
25. Horng, J.; Chen, C. F.; Geng, B.; Girit, C.; Zhang, Y.; Hao, Z.; Bechtel, H. A.; Martin, M.; Zettl, A.; Crommie, M. F.; *et al.* Drude Conductivity of Dirac Fermions in Graphene. *Phys. Rev. B* **2011**, *83*, 165113.
26. Rana, F. Graphene Terahertz Plasmon Oscillators. *IEEE Trans. Nanotechnol.* **2008**, *7*, 91–99.
27. Falkovsky, L. A.; Pershoguba, S. S. Optical Far-Infrared Properties of a Graphene Monolayer and Multilayer. *Phys. Rev. B* **2007**, *76*, 153410.

28. Gusynin, V. P.; Sharapov, S. G.; Carbotte, J. P. Magneto-optical Conductivity in Graphene. *J. Phys.: Condens. Matter* **2007**, *19*, 026222.
29. Hanson, G. W. Dyadic Green's Functions and Guided Surface Waves on Graphene. *J. Appl. Phys.* **2006**, *103*, 064302. Hanson, G. W. Quasi-TEM Modes Supported by a Graphene Parallel-Plate Waveguide. *J. Appl. Phys.* **2008**, *104*, 084314.
30. Hanson, G. W. Dyadic Green's Functions for an Anisotropic, Non-local Model of Biased Graphene. *IEEE Trans. Antenna Propagat.* **2008**, *56*, 747–757.
31. Mikhailov, S. A.; Ziegler, K. New Electromagnetic Mode in Graphene. *Phys. Rev. Lett.* **2007**, *99*, 016803.
32. Mishchenko, E. G.; Shytov, A. V.; Silvestrov, P. G. Guided Plasmons in Graphene p−n Junctions. *Phys. Rev. Lett.* **2010**, *104*, 156806.
33. Nair, R.; Blake, R. P.; Grigorenko, A. N.; Novoselov, K. S.; Booth, T. J.; Stauber, T.; Peres, N. M. R.; Geim, A. K. Fine Structure Constant Defines Visual Transparency of Graphene. *Science* **2008**, *320*, 1308.
34. Dawlaty, J. M.; Shivaraman, S.; Strait, J.; George, P.; Chandrashekhar, M.; Rana, F.; Spencer, M. G.; Veksler, D.; Chen, Y. Measurement of the Optical Absorption Spectra of Epitaxial Graphene from Terahertz to Visible. *Appl. Phys. Lett.* **2008**, *93*, 131905.
35. Chuang, F. T.; Chen, P. Y.; Cheng, T. C.; Chien, C. H.; Li, B. J. Improved Field Emission Properties of Thiolated Multi-wall Carbon Nanotubes on a Flexible Carbon Cloth Substrate. *Nanotechnology* **2007**, *18*, 395702.
36. Hu, J. Q.; Bando, Y.; Xu, F.; Li, Y.; Zhan, J.; Xu, J.; Golberg, D. Growth and Field-Emission Properties of Crystalline, Thin-Walled Carbon Microtubes. *Adv. Mater.* **2004**, *16*, 153–156.
37. Bhimarasetti, G; Cowley, J. M.; Sunkara, M. K. Carbon Microtubes: Tuning Internal Diameters and Conical Angles. *Nanotechnology* **2005**, *16*, S362.
38. Wang, R.; Hao, Y.; Wang, Z.; Gong, H.; Thong, J. T. L. Large-Diameter Graphene Nanotubes Synthesized Using Ni Nanowire Templates. *Nano Lett.* **2010**, *10*, 4844–4850.
39. Alù, A.; Rainwater, D.; Kerkhoff, A. Plasmonic Cloaking of Cylinders: Finite Length, Oblique Illumination and Cross-Polarization Coupling. *New J. Phys.* **2010**, *12*, 103028.
40. Kallos, E.; Argyropoulos, C.; Hao, Y.; Alù, A. Comparison of Frequency Responses of Cloaking Devices under Non-monochromatic Illumination. *Phys. Rev. B* **2011**in press.
41. Bohren, C. F.; Huffman, D. R. *Absorption and Scattering of Light by Small Particles*; Wiley: New York, 1998.
42. Papas, C. H. *Theory of Electromagnetic Wave Propagation*; Dover Publications: New York, 1988.
43. Abramowitz, M.; Stegun, I. A. *Handbook of Mathematical Functions with Formulas, Graphs, and Mathematical Tables*; Dover Publications: New York, 1972.